Research Article | Vol. 29, No. 4 / 15 February 2021 / Optics Express 6021

Optics EXPRESS

Two-wavelength phase-sensitive OTDR sensor using perfect periodic correlation codes for measurement range enhancement, noise reduction and fading compensation

MIKEL SAGUES,[1] ENRIQUE PIÑEIRO,[1] ENIS CERRI,[2] ALDO MINARDO,[2] AVISHAY EYAL,[3] AND ALAYN LOAYSSA[1,*]

[1] *Institute of Smart Cities and Department of Electrical, Electronic and Communications Engineering, Universidad Pública de Navarra, Pamplona, Spain*
[2] *Università della Campania Luigi Vanvitelli, Italy*
[3] *School of Electrical Engineering, Faculty of Engineering, Tel Aviv University, Tel Aviv, Israel*
[*] *alayn.loayssa@unavarra.es*

Abstract: We demonstrate a two-wavelength differential-phase-measuring OTDR sensor that uses perfect periodic correlation phase codes to enhance the measurement performance. The two-wavelength technique extends the measurement range of OTDR sensors by synthesizing a virtual longer-wavelength measurement from two simultaneous measurements of phase using different lasers. This increases the range free from phase unwrapping errors. However, we find that the application of this technique greatly increases the relative measurement noise. To compensate for this issue, we introduce the use of optical pulse compression using perfect periodic correlation phase codes to increase the measurement signal-to-noise ratio and also to facilitate the simultaneous compensation of Rayleigh and polarization fading. In addition, we apply a method to further reduce the relative noise that is added to the two-wavelength measurement by using the synthetic wavelength measurement to unwrap the differential phase measured with a single wavelength. All this is highlighted in a 1-km sensing link in which up to 20-cm spatial resolution and 12.6 $p\epsilon/\sqrt{Hz}$ strain sensitivity are demonstrated as well as a 67-fold enhancement in measurement range compared with the use of the conventional single-wavelength method.

1. Introduction

Distributed acoustic (vibration) sensing (DAS) based on reflectometric fiber optic techniques has recently received a great deal of attention due to its interesting applications in areas such as intrusion detection, seismic monitoring, structural health monitoring, or traffic monitoring [1]. A number of different methods have been developed to implement these sensors working either in the time or frequency domains [2,3]. Among them, phase-sensitive optical time-domain reflectometry (ϕ-OTDR) has been one of the most explored methods. Particularly, the so-called differential phase-measuring ϕ-OTDR ($d\phi$-OTDR), which can detect and quantify very small strain variations simply by measuring the optical phase difference of the backscattered light from contiguous locations in the fiber [1].

To date, the focus of research on $d\phi$-OTDR has been mainly on the high-precision applications that exploit the extreme sensitivity of these sensors. However, in principle, $d\phi$-OTDR sensors could also be deployed to provide measurements of the larger strain ranges normally associated with structural health monitoring (SHM) applications in fields such as civil engineering or condition monitoring of large machines such as wind turbines or electrical generators [4]. This would make $d\phi$-OTDR a simpler and better-performing alternative to dynamic Brillouin distributed sensors [5]. However, $d\phi$-OTDR sensors are intrinsically constrained by their phase-measuring nature and the associated need to deploy phase unwrapping methods. These

#413047 https://doi.org/10.1364/OE.413047
Journal © 2021 Received 22 Oct 2020; revised 14 Dec 2020; accepted 20 Dec 2020; published 10 Feb 2021

Optics EXPRESS

methods fail for large rates of strain change for which successive differences in phase change by more than π radians between samples, according to the so-called Itoh criterion [6]. This effect constrains the measurement range of the sensor, which is defined in the DAS context as the maximum amplitude of the vibration-induced strain that can be measured without distortion for a given vibration frequency [7,8]. Furthermore, it imposes the use of high temporal sampling frequencies even when the excitation of interest may be of a much lower frequency, as it is the case in most strain-measuring SHM applications.

We have recently demonstrated a method to overcome the π-phase constraint of $d\phi$-OTDR sensors by subtracting the differential phases measured for the two axes of a polarization-maintaining (PM) fiber [9]. The technique is based on making simultaneous measurements of the differential phase using two optical signals having slightly different wavenumber. The principle is similar to the so-called two-wavelength methods that have been used for years in digital holography [10] and interferometry [11], and that have been recently applied to DAS sensors too [12]. In these methods, the wavelength difference instead of refractive index difference is used to provide simultaneous measurement of the differential phase with two different wavenumbers. Thus, two lasers are used to synthesize a virtual longer-wavelength measurement for which the π-phase constraint is greatly relaxed.

In this paper, we investigate the application of two-wavelength methods to $d\phi$-OTDR and find that the relative noise of the measurement is greatly increased by the application of this technique. To compensate for this issue, we demonstrate the use of optical pulse compression (OPC) using perfect periodic correlation (PPC) phase codes to increase the measurement signal-to-noise ratio (SNR) and also to facilitate the simultaneous compensation of Rayleigh and polarization fading. In addition, we apply a method to further reduce the relative noise that is added to the two-wavelength measurement by making enhanced use of the measurement data provided by the two wavelengths. All this is highlighted in a 1-km sensing link in which 20-cm spatial resolution measurements with very large measurement range and strain rate are demonstrated.

2. Noise and fading in a two-wavelength $d\phi$-OTDR and its compensation

In a conventional $d\phi$-OTDR, the phase difference of the optical signals backscattered from two sections of the fiber, A and B, each with a length given by half the pulse duration and separated by the gauge length of the measurement, L, is given by [1]:

$$\Delta\phi = \frac{4\pi n}{\lambda}\xi\Delta L(t) + \vartheta_B - \vartheta_A = \Delta\varphi(t) + \vartheta \tag{1}$$

where n is the refractive index, λ is the wavelength of the optical source, $\Delta L(t)$ is the change in the gauge length induced by strain in the fiber, ξ is a correction to the optical path length change that accounts for the strain-optical effect, and ϑ_A and ϑ_B are the intrinsic random phase-shifts of the reflection from A and B. In (1), $\Delta\varphi(t)$ and $\vartheta \equiv \vartheta_B - \vartheta_A$ are defined in order to group the excitation and the intrinsic phase terms.

As explained in the introduction, the requirement for phase unwrapping imposes that the change of $\Delta\phi$ for successive measurements obtained by two consecutive pulses launched into the fiber is no greater than π radians. This was demonstrated by Itoh [6], which theoretically derived the necessary condition for exact tracking of phase differences from the definition of the wrapping and differentiating operators. This π-rad phase-difference threshold constrains the maximum amplitude of the strain that can be measured and the minimum pulse repetition frequency (slow-time sampling frequency) deployed. For instance, if we assume a sinusoidal excitation in the fiber with a frequency, f_e, the maximum amplitude of the strain that ensures that the phase-difference between successive temporal samples remains within the π-rad bound is

Optics EXPRESS

given by:

$$\epsilon_0 \approx \frac{\lambda}{8\pi n \xi L}\frac{f_s}{f_e} \tag{2}$$

where f_s is the slow-time sampling rate established by the period of the pulses launched into the fiber. This expression is derived simply by calculating the maximum slope of the phase-difference change for a sinusoid. Notice that there is a trade-off between the measurement range and the bandwidth of the measurement that is established by the π-phase constraint. This trade-off can be relaxed by increasing the temporal sampling rate, but this is limited in practice by the need to avoid the presence of more than one pulse in the fiber. Moreover, increasing the sampling rate to avoid the π-phase constraint beyond what is really demanded by the bandwidth of the excitation in the fiber, which tends to be small for SHM applications, translates to increased specifications for the measurement acquisition and processing subsystem of the sensor. This is not a minor issue for DAS systems that need to handle very large data throughput. Lastly, in systems where optical pulse compression is used to boost the SNR and the spatial resolution of the sensor, like the one that we are presenting in this paper, longer sequences are desirable because the compressed pulse amplitude is proportional to the energy of the sequence [13]. However, longer sequences mean a lower sampling rate, which, according to (2), compromises the measurement range.

Two-wavelength methods were proposed to mitigate the π-phase constraint in interferometry [11] and digital holography [10]. Their underlying idea is to perform the differential phase measurement simultaneously using two wavelengths, λ_1, λ_2, and substract the resultant phase shift differences to give:

$$\begin{aligned}\Delta\phi_S = \Delta\phi_1 - \Delta\phi_2 &= \frac{4\pi n}{\lambda_S}\xi\Delta L(t) + \left[\left(\vartheta_{B_1} - \vartheta_{A_1}\right) - \left(\vartheta_{B_2} - \vartheta_{A_2}\right)\right] \\ &= \Delta\varphi_S(t) + \vartheta_1 - \vartheta_2\end{aligned} \tag{3}$$

where $\lambda_S = \lambda_1\lambda_2/(\lambda_1 - \lambda_2)$ when dispersion is neglected. Again, $\Delta\varphi_S$ is defined in (3) to group the terms directly related to the phase difference between A and B induced by the fiber excitation, and ϑ_1 and ϑ_2 convey the intrinsic phase terms for each wavelength. Notice that $\Delta\varphi_S$ is equivalent to the differential phase that would be measured in a conventional $d\phi$-OTDR if the larger synthetic wavelength λ_S were used. This two-wavelength differential phase is reduced from the differential phase measured with any of the two single-wavelengths by a factor $M_1 = \Delta\varphi_1/\Delta\varphi_S = \lambda_2/|\lambda_1 - \lambda_2|$ and $M_2 = \Delta\varphi_2/\Delta\varphi_S = \lambda_1/|\lambda_1 - \lambda_2|$, respectively. This reduction in the sensitivity of the differential phase measurement leads to an equal increment of the measurement range, which, according to (2) is directly proportional to the wavelength used. Notice that if dispersion is taken into account and a different refractive index is considered for each wavelength, the derivation of a slightly more complex form of (3) and M_1 and M_2 is also straight forward.

However, the relaxed π-phase constrain for two-wavelength measurements comes at a cost. We have found that the relative noise of the measurement is greatly increased by this technique. The actually measured differential phase for each of the individual wavelength ($i = 1, 2$) when noise is taken into account is given by:

$$\widehat{\Delta\varphi_i} = \Delta\varphi_i(t) + \varphi_{n_i} \tag{5}$$

where φ_{n_i} is the noise added to the measurement. The hat operator ($\hat{}$) is used throughout this explanation to denote measured quantities with noise. Then, the SNR of the phase measurement, which we will call dynamic SNR (DSNR) following the convention in [14], is given by:

$$DSNR_i = \frac{\langle\Delta\varphi_i^2(t)\rangle}{\sigma_i^2} \tag{6}$$

Optics EXPRESS

where σ_i^2 is the variance of the noise term. As mentioned above, the phase difference measured with the synthetic wavelength is a scaled version of that measured with the individual wavelengths, $\Delta\varphi_S = \Delta\varphi_i/M_i$. Therefore, the DSNR for the synthetic wavelength measurement can be calculated as:

$$DSNR_S = \frac{\langle \Delta\varphi_i^2(t) \rangle}{2M_i^2\sigma_i^2} \tag{7}$$

Notice that there is a $2M_i^2$ penalty in the measurement DSNR compared with those for the individual wavelengths that is due to the fact that the noise of the individual wavelengths adds in the combined two-wavelength measurement and it is not scaled as the differential phase. This penalty introduces a serious degradation in the sensor performance as highlighted in the experimental section of this paper.

2.1. Noise compensation in a two-wavelength $d\phi$-OTDR

We propose the application of a simple method to compensate the noise penalty in two-wavelength $d\phi$-OTDR sensors. This is also based on principles that were first proposed in two-wavelength digital holography [15]. The fundamental idea behind the method is to take advantage of the synthetic wavelength measurement, which is free from the π-phase constrain, to unwrap the measurements of the individual wavelength measurements. The differential phase in (1) can be expressed as:

$$\Delta\varphi_i = \Delta\dot{\varphi}_i + 2\pi k_i \tag{8}$$

where $\Delta\dot{\varphi}_i$ represents the actual wrapped phase that is measured in the ideal $d\phi$-OTDR receiver and k_i is an integer that gives the fringe order of the total phase difference. Then, assuming that we can measure the unwrapped two-wavelength phase difference, $\widehat{\Delta\varphi_S}$, the fringe order for one of the individual wavelength measurements, $\Delta\dot{\varphi}_i$, can be calculated by:

$$\widehat{k_i} = round\left(\frac{\widehat{\Delta\varphi_S}M_i - \widehat{\Delta\dot{\varphi}_i}}{2\pi}\right) \tag{9}$$

with $\widehat{\Delta\dot{\varphi}_i}$ the measured wrapped differential phase for one of the wavelengths. Notice, that, basically, what the method does is to re-scale $\widehat{\Delta\varphi_S}$ and use it to determine the fringe order of $\Delta\varphi_i$. Once this is done, the differential phase measurement, and from it the strain measurement of interest, can be retrieved with an unwrapped version of $\Delta\varphi_i$ that does not face the π-phase constrain and has the DSNR of the single-wavelength measurement as in (5).

However, (8) is free from phase wrapping errors just up to a certain level of noise in $\widehat{\Delta\varphi_S}$. Indeed, if we separately consider added noise, (8) becomes:

$$\widehat{k_i} = round\left(\frac{\Delta\varphi_S M_i - \Delta\dot{\varphi}_i}{2\pi} + \frac{\varphi_{n_S}M_i - \varphi_{n_i}}{2\pi}\right) \tag{10}$$

The first term within the round operator is the ideal result, which gives the integer fringe order. The second term is the added noise, which, to avoid errors in the determination of the order, should be smaller than $\pm 1/2$. For instance, we can set a 3-σ limit for the noise, i.e. limit three times the standard deviation of the noise term in (9) to be smaller than 1/2 (3σ<1/2). This ensures that (9) gives the correct result 99.73% of the time. In this case, the allowable standard deviation of the noise for each wavelength is given by:

$$\sigma_i < \frac{2\pi}{6\sqrt{2}M_i} \tag{11}$$

In practical deployments, achieving the level of noise required by (10) is difficult, particularly if long lengths of sensing fiber are deployed and a good spatial resolution is necessary. This

Optics EXPRESS

is where PPC OPC comes into play. OPC is a method borrowed from radar in which pulses with a broadened spectra are compressed using a matched filter to increase the SNR and spatial resolution of measurements [16,17]. PPC are an enhanced type of phase codes used for OPC that have been already demonstrated to greatly increase the SNR and the spatial resolution in $d\phi$-OTDR sensors [9,18]. The main advantages for this application of PPC OPC compared to the more conventional OPC deploying linear frequency-modulated (LFM) pulses is, firstly, the reduction of sidelobes in the compressed pulse, which are nonexistent in ideal PPC OPC, and, secondly, the simplicity of the generation and tuning of these sequences. The PPC sequence can be generated by modulation of the phase of an optical carrier using a simple setup based on a Mach-Zehnder electro-optic modulator (MZ-EOM) biased at minimum transmission [9]. Moreover, the pulse compression, and with it, the spatial resolution, can be enhanced simply by reducing the duration of the individual bits in the sequence. The use of PPC OPC is also advantageous compared with the use of other codes such as Golay codes that require the injection in the fiber of four complementary code sequences and provide a lower coding gain.

We propose the use of PPC OPC in two-wavelength $d\phi$-OTDR sensors to achieve the performance levels required to increase the DSNR of the synthetic wavelength measurement (6), partially compensating the incurred penalty, and even reaching the low noise levels required to apply the fringe order determination technique that we propose. Furthermore, the combination of PPC OPC and two-wavelengths measurements is particularly advantageous because the use of the synthetic wavelength measurement, as it has been explained, relaxes the requirement on the slow-time sampling rate. Therefore, longer PPC sequences can be used which translates into an increased SNR because the amplitude of the compressed signal is proportional to the PPC sequence energy.

2.2. Fading compensation

Another system issue of two-wavelength $d\phi$-OTDR sensors whose solution can be facilitated by the use of PPC OPC is that of the signal fading due to the destructive interference of the backscattered signals within a pulse-length. This fading probability follows the Rayleigh distribution and corrupts the phase measurement when the signal amplitude is so small as to be contaminated by noise.

The most common method to compensate for fading in $d\phi$-OTDR sensor setups is to make use of wavelength diversity to obtain several measurements that are sufficiently uncorrelated [19]. The implementation of this principle has been demonstrated with simpler schemes using simultaneous pulses of different frequencies [20,21], and, more recently, also embedded within sensors employing LFM OPC [22,23]. In every case, the need to accommodate the multiple frequencies translates to either an increase in the required receiver and acquisition system signal bandwidth or in a reduced spatial resolution if bandwidth is maintained. This is traded-off for fading compensation.

Here, we deploy another fading compensation method that takes advantage of PPC OPC and that offers similar trade-offs to the multiple-frequency methods but with a simpler implementation in the spatial domain. What we do is simply to increase the spatial resolution of the measurement by reducing the duration of the bit of the PPC sequence. If we reduce the duration of the bit by an integer factor N, the spatial resolution is increased by N. Then, we can use the increased number of measurements provided by the compression, which are uncorrelated as they come from non-overlapping locations of the compressed pulse, in much the same way that with measurements with multiple frequencies. Moreover, the penalty for the fading compensation with this technique is similar to the use of multiple frequencies, as the reduction in the duration of the pulse leads to a factor of N increase in the received signal bandwidth.

In order to take advantage of the measurement diversity provided by this technique, the rotated-vector-sum method can be applied [22], followed by a moving average with a window equivalent

Optics EXPRESS

to N pulse-lengths in the fiber. Nevertheless, other methods of combining the independent measurements provided by the method are possible [24]. In any case, it has been shown that just using $N = 3$ would be enough, by and large, to compensate fading. However, larger factors can be used to further increase the SNR, as will be shown in the experiments section.

Finally, the use of two wavelengths in $d\phi$-OTDR sensors also provides a simple method to compensate polarization fading. This fading is the result of the mismatch between the state of polarization (SOP) of the local oscillator used in the coherent detection used to obtain full phase information of the optical field and the SOP of the backscattered signals from certain locations in the fiber. The standard method to compensate this fading is to use receivers with polarization diversity [25]. However, the use of the synthetic wavelength measurement, and the already mentioned relaxation in the requirement for slow-time sampling rate, provides the opportunity to deploy a much simpler polarization switching in which consecutive measurements with orthogonal polarization of the optical signals launched into the fiber are performed. Inexpensive polarization switches, typically based on the Faraday effect, are available. These devices have switching times of several tens of microseconds that are impossible to handle by single-wavelength $d\phi$-OTDR because of the π-phase constraint associated with such a large sampling period. On the contrary, they can be deployed when using the synthetic wavelength measurement because the technique provides enough time between consecutive pulses to rotate the SOP.

3. Experimental setup

Figure 1 depicts the experimental setup used to demonstrate our two-wavelength $d\phi$-OTDR sensor. This is basically a $d\phi$-OTDR sensor in which PPC coding and a second laser are added. The outputs of two lasers at λ_1=1551.72 nm and λ_2=1530.33 nm are split into two branches each. The linewidth of the two lasers was 0.1 kHz and 2.1 kHz, respectively. One branch is directly connected to the local oscillator input of a homodyne receiver that comprises a 90° optical hybrid and two balanced detectors.

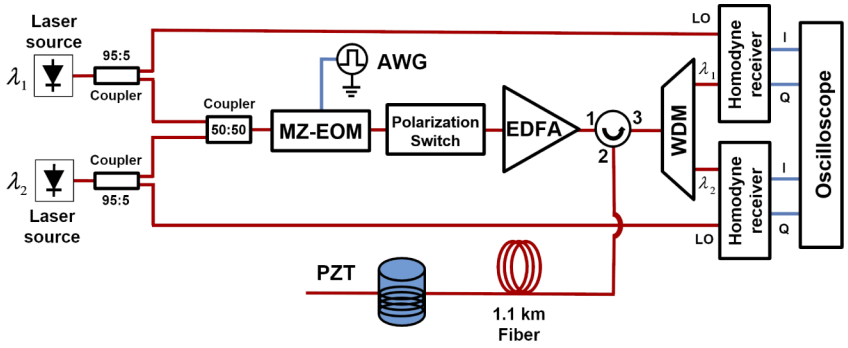

Fig. 1. Experimental setup of the two-wavelength phase-measuring $d\phi$-OTDR sensor.

The other two branches are combined and fed to a Mach-Zehnder electrooptic modulator (MZ-EOM). The MZ-EOM is of the push-pull type, in which opposite phase-shifts are applied to the two arms of the interferometer, and it is biased at the minimum transmission. This makes the modulator generate a pure BPSK modulation in response to the applied voltage [9]. The PPC sequence signal applied to the modulator is generated in an arbitrary waveform generator (AWG) and then amplified in a driver. At the output of the MZ-EOM, a polarization switch with a switching time of approximately 100 μs is used to obtain polarization diversity in successive sequences. The PPC sequences are constantly generated by the AWG and the switching of the polarization switch is synchronized so that all the measured backscattered signals from a single

Optics EXPRESS

sequence are received with stable polarization. Notice that both λ_1 and λ_2 were well within the operating wavelength range of the MZ-EOM and the polarization switch.

Then, the optical signal from the polarization switch is amplified in an EDFA and launched into the sensing fiber. The two wavelengths present in the signal backscattered from the fiber are separated using a wavelength demultiplexer (WDM) and sent to their respective receiver. Finally, the received electrical signals are digitized in a 4-channel scope and processed on a computer.

The sensing fiber link was made of a 1.1-km length of standard single-mode fiber. At the far end of the fiber, a 10-m piezoelectric fiber stretcher (PZT) is used to introduce dynamic strain.

4. Experimental results

First, we analyze the pulse compression obtained with the PPC coding. Figure 2 depicts the autocorrelation of the detected signal measured by directly connecting the output of the MZ-EOM to the homodyne receiver. This is the measurement for the λ_1 channel, but, apart from the background noise, it is identical for both channels. The duration of each bit of the deployed PPC code was 2.5 ns with a code length of 52027 for a total duration of 130 μs for the sequence. Figure 2(b) shows the detail of the PPC compression peak where a spatial resolution of approximately 20 cm is measured for the full-width half-maximum amplitude (−6dB). Also displayed in Fig. 2 is the theoretical autocorrelation of an LFM wave with a passband bandwidth equal to that of the PPC sequence (approx. 800 MHz). This figure highlights the advantage of using PPC codes compared to OPC based on the more conventional linear frequency modulated (LFM) waveforms. Ideally, the PPC should have no sidelobes. However, a couple of small sidelobes that are 29 dB below the peak are visible. After performing some simulations of the effect of a nonlinear transfer function on pulse compression, the existence of these sidelobes was attributed to the nonlinear distortion introduced by the driver feeding the MZ-EOM. Therefore, they could be suppressed in principle by devising a pre-distortion of the generated code sequence signal. However, this is outside the scope of this work. Nevertheless, it can be seen that the sidelobe amplitude is 13-dB lower than the sidelobes present in LFM compression, hence, their effect in terms of degradation of the spatial resolution and cross-talk between measurements from closely-spaced excitation can be neglected. Notice that the crosstalk of the measurement in one position of the fiber on another closely spaced position just depends on the relative amplitude of the compressed backscattered signals from both locations. Therefore, a sidelobe 29 dB below a backscattered signal would only affect nearby signals that were already experiencing a high fading that would have to be compensated anyway.

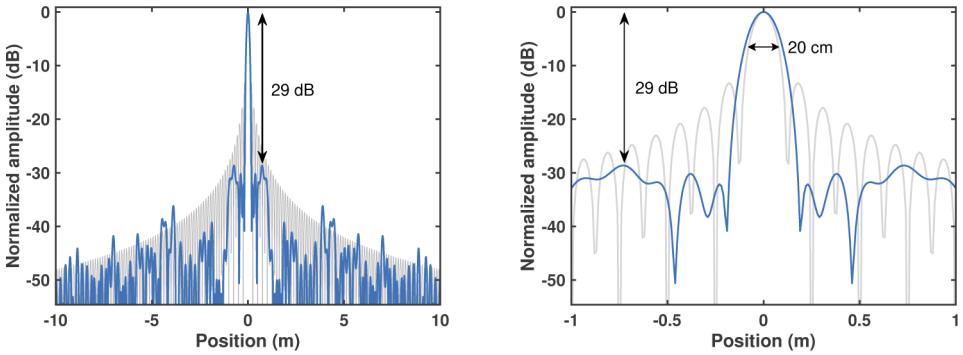

Fig. 2. (a) Measured pulse compression with a PPC sequence of 2.5-ns bit duration and 52027-bit length (blue line) and theoretical compression of an 800-MHz bandwidth LFM signal (grey line). (b) Expanded view of (a) around the autocorrelation peak.

Optics EXPRESS

Next, we demonstrate the fading compensation method taking advantage of the high resolution provided by PPC coding. Figure 3(a) depicts the received signal for one of the wavelengths after matched filtering and pulse compression. A great number of signal fadings can be observed. The differential phase measurement at those low-amplitude locations is contaminated by the random phase of the noise floor. The histogram on the side depicts the distribution for the signal amplitude, which follows a Rayleigh profile as expected. Figure 3(b) shows the same signal after vector rotation and moving average has been applied with a window length equivalent to 3 pulse-lengths, which, in this case, is 3×25 cm. Hence, the spatial resolution is slightly reduced to 0.75 m. We can see that this simple processing is enough to suppress most fadings. Notice that in the histogram of amplitudes the values close to zero are suppressed. Figure 3(c) displays the same process but extending the window length to 20 pulse-lengths, which translates to a final spatial resolution of the resultant measurement of 5 m. We see that the distribution of amplitudes is further migrating from a Rayleigh to a normal distribution. Besides, we can see in the trace outside the fiber that the noise is reducing its amplitude as a result of the window averaging. Hence, the SNR of the measurement is improved. This is confirmed in Fig. 3(d) where the static SNR of the measurement as a function of the number of equivalent pulse-lengths in the moving average is shown. This enhanced SNR is traded-off for a reduction in the spatial resolution. It must be pointed out that the moving average does not alter the differential phase measurements obtained in the $d\phi$-OTDR sensor because in the applied rotated-vector-sum algorithm the initial optical phase for the compressed backscattered signal from all positions in the sensing fiber is rotated to a common angle [22].

Figure 4(a) highlights the polarization fading compensation that is achieved with the use of the polarization switch. Two groups of compressed backscattering traces, which correspond to the two orthogonal SOP launched into the fiber for alternating measurements, are depicted. Notice that there are positions along the fiber in which the amplitude for one of the polarizations is very small whereas the other polarization displays a reasonable amplitude. These positions correspond to areas of polarization fading for one of the SOPs. If it were not for the availability of another measurement with orthogonal SOP, the measurement from those locations would be contaminated by noise leading to high noise on the recovered phase difference measurements. On the contrary, there are locations where both polarizations have a small amplitude. In these cases, the fading is due to the destructive interference from the set of backscattered optical signals received from the pulse length corresponding to those locations. This fading needs to be compensated by other methods such as the moving average technique described above.

Figure 4(b) demonstrates the effect of the use of polarization diversity on the measurements performed with a single wavelength. The standard deviation of the slow-time differential phase measured for a section of the fiber that was enclosed in an acoustic isolation box to prevent any excitation is depicted. The polarization fading compensation strategy that has been deployed for these measurements is to keep the measurement with the highest amplitude at each position, although other options are possible. Notice that this strategy reduces the overall noise of the measurement compared to the use of any of the single-polarization measurements.

Figure 5(a) depicts the differential phase measurements obtained in the fiber stretcher, which was excited with a sine wave of 25-Hz frequency and 60-V amplitude. Note that the excitation frequencies used throughout this work are in the tens of hertz order because those are typical of the SHM of large structures in which the two-wavelength method has its primary application. The two single-wavelength measurements as well as the synthetic wavelength measurement are depicted. A 10427 code length with a bit duration of 2.5 ns and a total sequence duration of 26 μs was used in these measurements. The slow-time sampling period was set to 156 μs to give time to the polarization switch to transition between polarization states in polarization diversity measurements. Notice that the synthetic wavelength measurement uses the right vertical axis with a different scale to account for the phase reduction factor associated with this measurement.

Optics EXPRESS

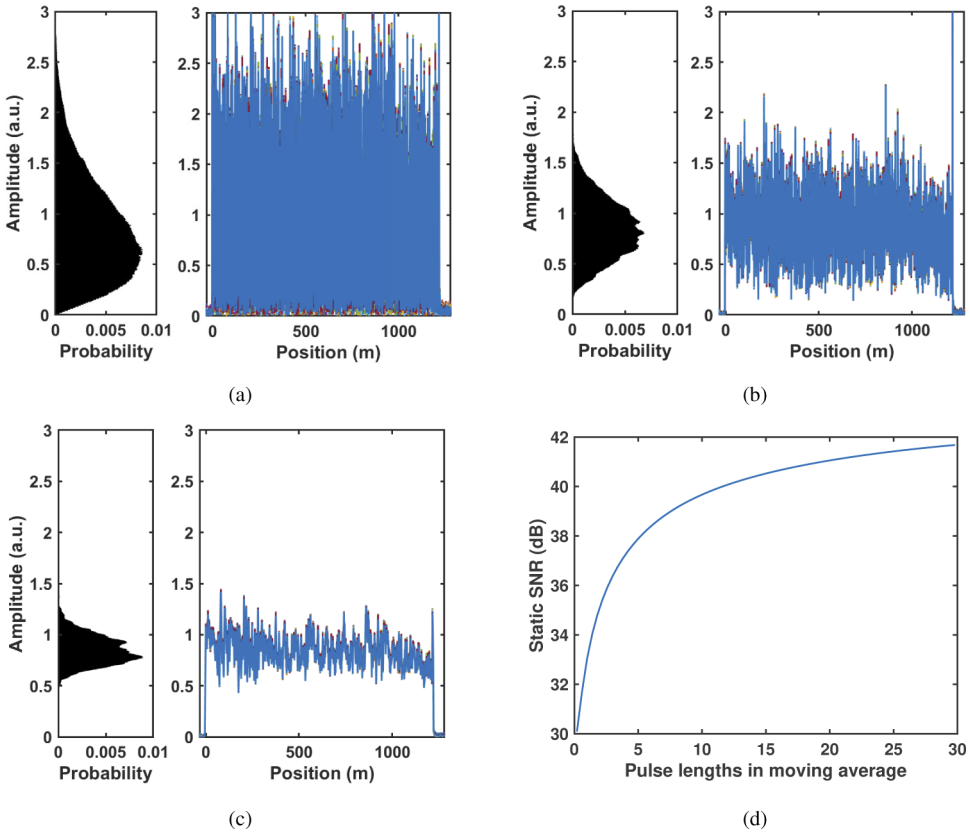

Fig. 3. Fading compensation based on PPC compression with (a) no moving average and with averaging of (b) 3 pulse-lengths and (c) 20 pulse-lengths. (d) Static SNR as a function of the number of equivalent pulse-lengths in the moving average.

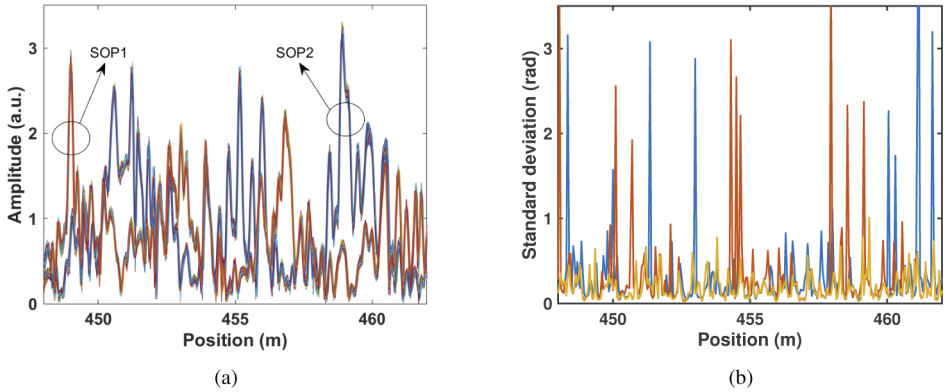

Fig. 4. Experimental results for the polarization diversity technique. (a) Amplitude of the detected signal for each of the two orthogonal states of polarization (SOP1 and SOP2) of the light launched into the fiber. (b) Standard deviation of the phase for each state of polarization (blue and red lines) and for the result of applying the polarization diversity strategy (yellow line).

Optics EXPRESS

The synthetic wavelength, given the values of λ_1 and λ_2, is 111 μm. Hence, the scale factors are $M_1 \approx 72.5$ and $M_2 \approx 71.5$, respectively. The gauge length for these measurements was set to 20 m so as to include all the phase change induced by the 10-m stretcher. A 3-pulse-length moving average was implemented to compensate fadings as described above. Figure 5(b) depicts the strain calculated from the three phase measurements using (1). The strain measured by the three measurements is identical, but notice the increased noise in the synthetic wavelength measurement. In fact, the DSNR measured for the single-wavelength traces by taking a fast Fourier transform was 86 dB above the noise floor, and for the synthetic wavelength measurement was 43 dB. This confirms a DSNR penalty approximately equal to the 40 dB theoretically predicted by (6).

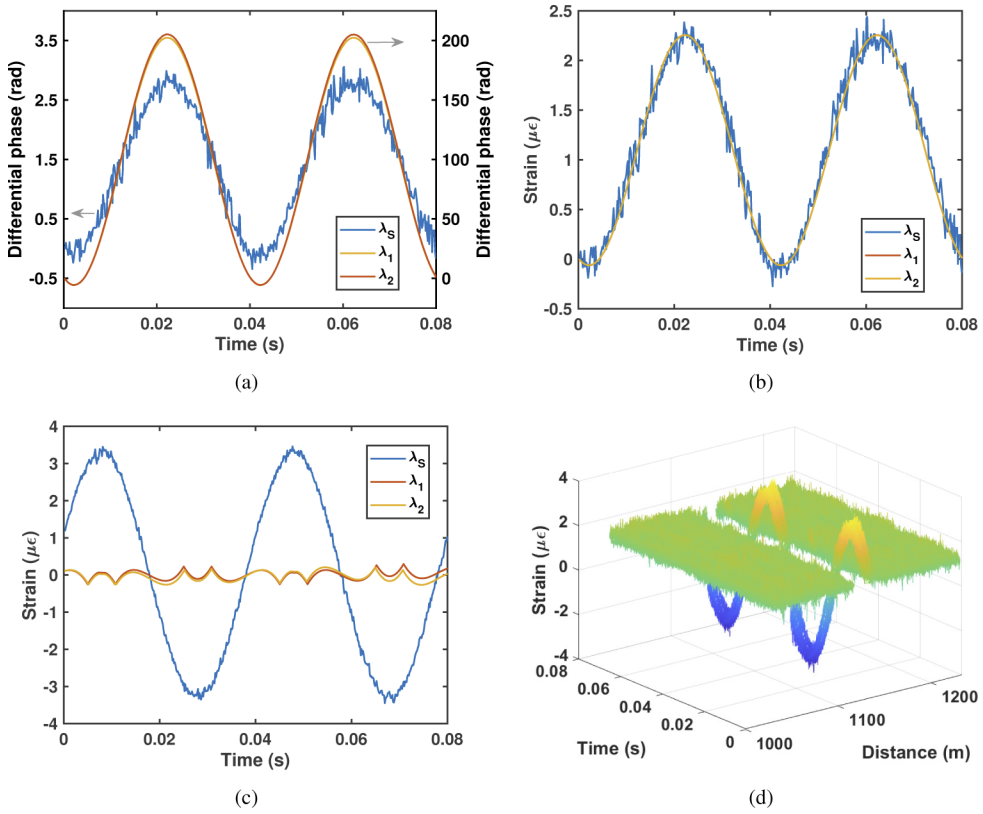

Fig. 5. Measurement of differential phase and strain in the piezoelectric fiber stretcher for a 25-Hz sinusoidal excitation: single-wavelength (red and yellow lines) and synthetic wavelength (blue line) measurements of (a) differential phase and (b) strain for 60-V amplitude of the excitation, (c) strain measurements for 170-V amplitude of the excitation, and (d) distribution of the strain measurements at the position of the fiber stretcher and its vicinity.

Obviously, in the measurement scenario depicted in Fig. 5(a) and Fig. 5(b), it would make little sense to deploy the two-wavelength method because any of the conventional single-wavelength measurements provides the correct measurement with much less noise. In fact, that is precisely the way this sensor would work in practice: upon performing a measurement, first, the synthetic-wavelength differential-phase measurement, after proper scaling, would be used to determine whether a particular excitation is below the rate of phase change that can be handled by the single-wavelength measurements according to the threshold defined by (2). If that is the case as in Fig. 5(a), the strain measurement would proceed by using the single-wavelength measurement

Optics EXPRESS

to obtain the low-noise strain measurement in Fig. 5(b). However, the situation changes if a higher strain is induced in the fiber stretcher by increasing the applied voltage to 170 V as depicted in Fig. 5(c). This increment is enough to pass the threshold defined by (2) and make the single-wavelength measurement to incur errors in the phase unwrapping because the phase difference between consecutive measurements changes by more than π rad. In such a high strain scenario the single-wavelength measurements can no longer be trusted. However, we can see that the synthetic wavelength measurement still provides a correct measurement. Furthermore, Fig. 5(d) depicts the distribution of the synthetic wavelength measurements at the position of the fiber stretcher and its vicinity demonstrating the correct localization and quantification of vibration amplitudes beyond the capabilities of standard single-wavelength phase-measuring distributed vibration sensors.

Figure 6(a) depicts the dependence of the measured strain amplitude on the applied PZT excitation for the sensor parameters used in Fig. 5. Notice that the response is linear for single-wavelength as well as synthetic wavelength measurements for the lower part of the amplitude range. However, from 65 V the single-wavelength measurement breaks because it crosses the π-phase threshold, as it was highlighted in Fig. 5(c), and depart from linearity giving a wrong response. The synthetic wavelength measurement, by contrast, remains linear throughout the excitation range. Figure 6(b) and Fig. 6(c) display identical measurements to Fig. 6(a) but for excitation frequencies of 12.5 Hz and 50 Hz, respectively. Notice that the higher the frequency, the lower the maximum amplitude that can be measured by the single-wavelength sensors before breaking, which are approximately 130 V and 32.5 V for the 12.5-Hz and 50-Hz frequencies, respectively. In fact, the amplitude threshold directly scales with the inverse of the excitation frequency as predicted by (2). By increasing the excitation frequency, we are increasing the differential phase change rate so that the maximum amplitude that can be measured without phase unwrapping errors reduces. Finally, Fig. 6(d) shows the measurement for 25-Hz excitation but increasing the slow-time sampling period to 4 ms. This gives a reasonable f_s=250 Hz of sampling frequency, which is enough to follow the time-domain evolution of a 25-Hz signal without the unnecessarily high number of samples provided by the f_s = 6.4 kHz in the other measurements. The single-wavelength measurements for these conditions give wrong results from 2.5 V, as calculated from (2), whereas the two-wavelength measurement reaches 170 V. This means that our two-wavelength system is demonstrating an approximately 67-fold enhancement in the measurement range of the $d\phi$-OTDR sensor, which is defined as the maximum amplitude of the vibration-induced strain that can be measured by a DAS without distortion for a given vibration frequency [7,8]. This is close to the theoretical limit of measurement range enhancement which would be equal to the scale factor $M_2 \approx 71.5$.

Once the improvement in measurement range provided by the two-wavelength $d\phi$-OTDR method has been highlighted, we focus on demonstrating the methods that we propose to compensate the noise added by the application of the technique. Figure 7(a) depicts the strain measurement in the PZT location using the same sensor parameters as in Fig. 5, but reducing the amplitude of the strain excitation in the PZT an order of magnitude to 15 V. In addition, the slow-time sampling period was set to 1.17 μs, which gives a comfortable 854-Hz sampling frequency. Notice that the reduction of the measured excitation makes the noise in the measurement even more visible. The DSNR for the synthetic wavelength measurement was 25 dB above the FFT noise floor. Moreover, we can not resort to the single-wavelength measurements for a lower-noise measurement because they are already broken due to the phase-unwrapping errors.

Figure 7(b) highlights the first method that can be used to reduce the noise, which is to increase the length of the PPC sequence to increase its energy. In this case, it was extended to 52027 bits for a total duration of 130 μs. The increased energy of the PPC sequence leads to an increment of the DSNR obtained after matched filtering, which reaches 31 dB. This improvement could be made larger by further increasing the sequence length. One limit to this improvement would be

Optics EXPRESS

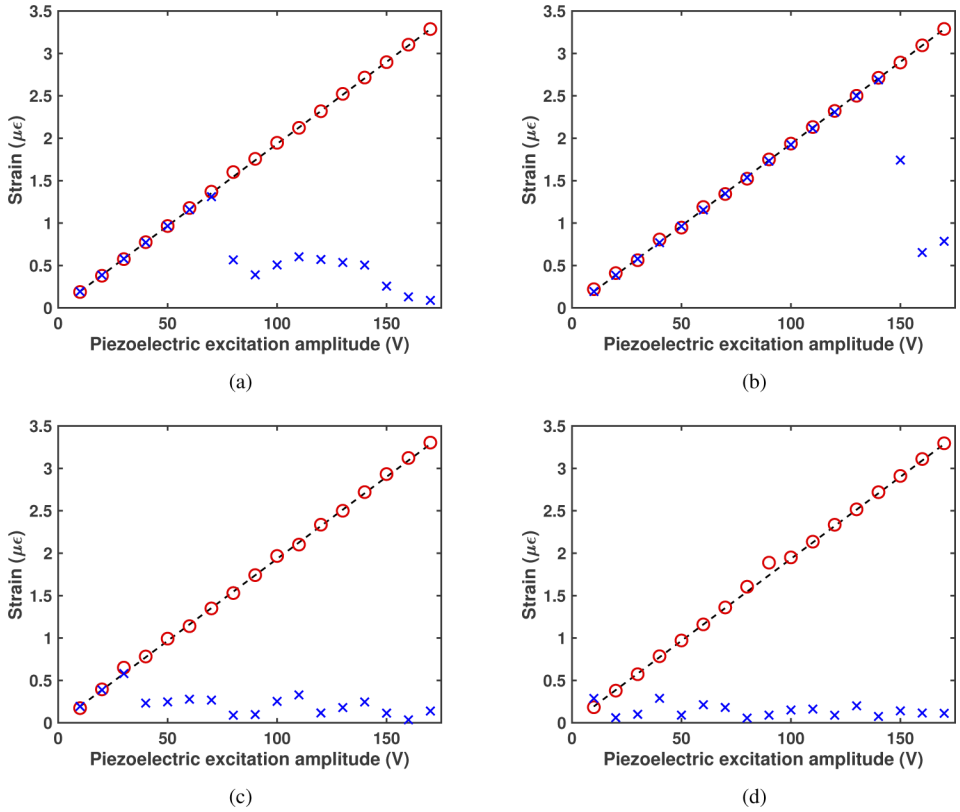

Fig. 6. Response of the two-wavelength $d\phi$-OTDR sensor strain measurement as a function of the amplitude of the excitation in the piezoelectric fiber stretcher for excitation frequencies of (a) $f_e = 25$ Hz, (b) $f_e = 12.5$ Hz, and (c)$f_e = 50$ Hz, with a sampling frequency of $f_s = 6.4$ kHz, and (d) for excitation frequency of $f_e = 25$ Hz with a sampling frequency of $f_s = 250$ Hz. Both the two-wavelength (red circles) and single-wavelength (blue crosses) measurements are shown, along with the theoretical response (black dashed-line)

to ensure that the resultant reduced slow-time sampling rate as a result of the increased sequence length does not compromise the measurement range in accordance with (2). The other issue to consider is the effect that phase noise may have in terms of added noise or degraded spatial resolution, which needs to be further studied. However, in our proof-of-concept experiments, the limiting factor to further increase the sequence length and with it the SNR was the storage memory of the digital oscilloscope that was used to capture the signal. Due to this limitation, we had to resort to the other strategy outlined in section 2 to increase the SNR by increasing the moving average window to 30 pulse-lengths. This gave the measurement in Fig. 7(c). The DSNR of this measurement raises to 38.5 dB. Notice that this cleaner signal is obtained at the price of reducing the spatial resolution to 7.5 m.

Once the noise of the measured signal was small enough, the fringe order determination method described in section 2.1 could be applied. Figure 7(d) depicts the single-wavelength wrapped differential phase measured and the fringe order calculation obtained using (8) with the synthetic wavelength measurement in Fig. 7(c). This calculation is finally used to unwrap the single-wavelength measurement and obtain the strain measurement depicted in Fig. 7(e), which highlights the complete compensation of the noise added due to the two-wavelength method. This is confirmed in Fig. 7(f), which depicts the spectral density of the strain before (measurement in

Optics EXPRESS

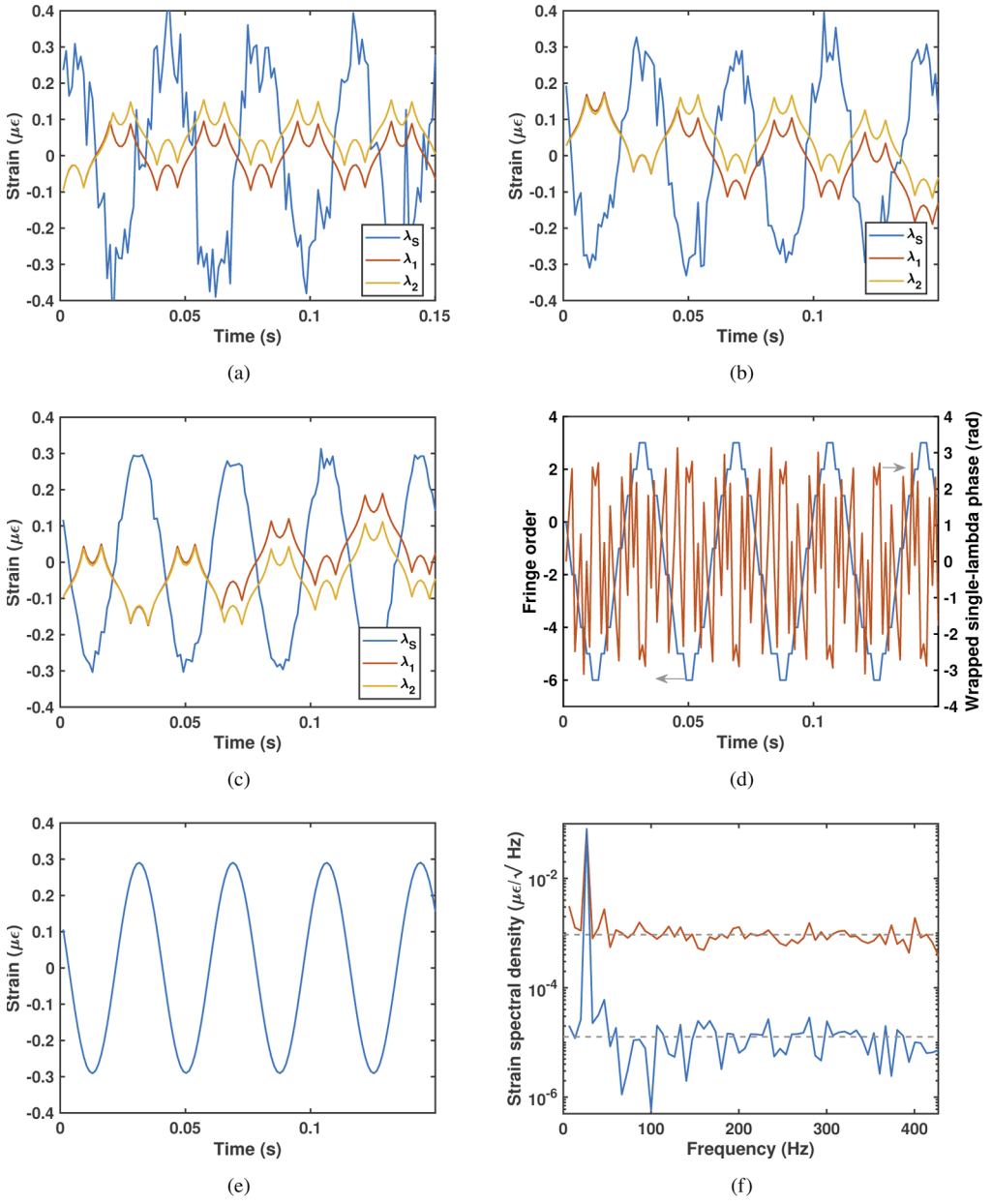

Fig. 7. Measurement of strain in the piezoelectric fiber stretcher for excitation amplitude of 15 V and demonstration of the noise compensation method: (a) Measurement with 10427-bit PPC code length and 3-pulse-length moving average, (b) measurement extending the PPC code length to 52027 bits, (c) measurement increasing the moving average window to a 30 pulse-length window, (d) application of the fringe-order determination technique, (e) compensation of the synthetic wavelength noise using the fringe-order method, and (f) spectral density of the measured strain before (red line) and after (blue line) application of the fringe-order noise compensation method.

Optics EXPRESS

Fig. 7(c)) and after (measurement in Fig. 7(e)) applying the noise compensation method. The DSNR of the final measurement increases to 76 dB and the sensitivity reaches 12.6 $p\epsilon/\sqrt{Hz}$. This later value is directly obtained from the measured noise floor in Fig. 7(f), which is already expressed in units of spectral density of strain.

5. Conclusions

We have demonstrated that the application of the two-wavelength method to $d\phi$-OTDR sensors serves to greatly extend their measurement range making them suitable for applications in SHM where high strain ranges are expected. Moreover, we have studied in detail the measurement performance of these sensors, particularly the noise penalty incurred by the method, and have proposed techniques to overcome its degradation. Proof-of-concept experiments have been used to demonstrate these techniques, but to obtain the ultimate performance of the sensor a series of modifications in the sensor setup would be desirable. First of all, it is the issue of choosing wavelengths. In our case, the deployed wavelengths were determined by the lasers that we had available, but, depending on the application, it would be more interesting to choose another set of wavelengths. In our setup, the wavelengths are relatively close and this leads to a very large resultant synthetic wavelength, which is good because the strain range without phase wrapping errors due to the π-phase constrain is very large. However, the SNR penalty is also large and this complicates achieving the minimum noise level required to apply the fringe order determination technique in (8). In practice, more widely spaced wavelengths would be desirable to reduce the SNR penalty. The synthetic wavelength would be also reduced in this case, which could compromise the achievable measurement range enhancement according to (2). However, there is still room to increase the measurement range by applying techniques that have been used for this purpose in two-wavelength interferometry and digital holography [26,27]. The other issue of the setup, which is common to all $d\phi$-OTDR sensors, is that of the linearity of the measurements. All the derivations in this paper assume that ϑ_B and ϑ_A, the intrinsic phase from the reflections from the two extremes of the gauge length, are approximately constant. However, in a system in which there are large strains in those positions this assumption would be invalid, which would break the measurements. Therefore, $d\phi$-OTDR sensors are really more suitable for application in quasi-distributed measurements in which there are point reflection areas along the fiber. A particularly convenient and cost-effective arrangement would be to deploy a fiber with localized reflectors induced through the cladding using a laser [28].

Funding. Agencia Estatal de Investigación (PID2019-107270RB-C22).

Disclosures. The authors declare no conflicts of interest.

References

1. A. Hartog, *An Introduction to Distributed Optical Fibre Sensors*, Fiber Optic Sensors (Taylor & Francis Group, 2018).
2. Z. Ding, C. Wang, K. Liu, J. Jiang, D. Yang, G. Pan, Z. Pu, and T. Liu, "Distributed optical fiber sensors based on optical frequency domain reflectometry: A review," Sensors **18**(4), 1072 (2018).
3. R. Zinsou, X. Liu, Y. Wang, J. Zhang, Y. Wang, and B. Jin, "Recent progress in the performance enhancement of phase-sensitive otdr vibration sensing systems," Sensors **19**(7), 1709 (2019).
4. A. Loayssa, "Structural health monitoring using distributed fibre optic sensors," in *Optical Fibre Sensors: Fundamentals for Development of Optimized Devices*, (IEEE, 2021), chap. 5, pp. 125–149.
5. A. Masoudi and T. P. Newson, "Contributed review: Distributed optical fibre dynamic strain sensing," Rev. Sci. Instrum. **87**(1), 011501 (2016).
6. K. Itoh, "Analysis of the phase unwrapping algorithm," Appl. Opt. **21**(14), 2470 (1982).
7. IEC 61757-3-2, "Fibre Optic Sensors - Part 3-2: Acoustic sensing - Distributed sensing," Draft standard, International Electrotechnical Commission, Geneva, CH (2020).
8. SEAFOM MSP-02, "Measuring Sensor Performance: DAS Parameter Definitions and Tests," Tech. rep., SEAFOM international Joint Industry Forum (2018).

Optics EXPRESS

9. J. J. Mompó, L. Shiloh, N. Arbel, N. Levanon, A. Loayssa, and A. Eyal, "Distributed dynamic strain sensing via perfect periodic coherent codes and a polarization diversity receiver," J. Lightwave Technol. **37**(18), 4597–4602 (2019).
10. J. C. Wyant, "Testing aspherics using two-wavelength holography," Appl. Opt. **10**(9), 2113–2118 (1971).
11. C. Polhemus, "Two-wavelength interferometry," Appl. Opt. **12**(9), 2071–2074 (1973).
12. H. He, L. Yan, H. Qian, X. Zhang, B. Luo, and W. Pan, "Enhanced range of the dynamic strain measurement in phase-sensitive otdr with tunable sensitivity," Opt. Express **28**(1), 226–237 (2020).
13. J. J. Mompó, S. Martín-López, M. González-Herráez, and A. Loayssa, "Sidelobe apodization in optical pulse compression reflectometry for fiber optic distributed acoustic sensing," Opt. Lett. **43**(7), 1499–1502 (2018).
14. H. Gabai and A. Eyal, "On the sensitivity of distributed acoustic sensing," Opt. Lett. **41**(24), 5648–5651 (2016).
15. D. Parshall and M. K. Kim, "Digital holographic microscopy with dual-wavelength phase unwrapping," Appl. Opt. **45**(3), 451–459 (2006).
16. S. Wang, X. Fan, Q. Liu, and Z. He, "Distributed fiber-optic vibration sensing based on phase extraction from time-gated digital OFDR," Opt. Express **23**(26), 33301 (2015).
17. W. Zou, S. Yang, X. Long, and J. Chen, "Optical pulse compression reflectometry: proposal and proof-of-concept experiment," Opt. Express **23**(1), 512 (2015).
18. L. Shiloh, N. Levanon, and A. Eyal, "Highly-sensitive distributed dynamic strain sensing via perfect periodic coherent codes," in *26th International Conference on Optical Fiber Sensors*, (Optical Society of America, 2018), p. TuE25.
19. M. D. Mermelstein, R. Posey, G. A. Johnson, and S. T. Vohra, "Rayleigh scattering optical frequency correlation in a single-mode optical fiber," Opt. Lett. **26**(2), 58–60 (2001).
20. J. Zhou, Z. Pan, Q. Ye, H. Cai, R. Qu, and Z. Fang, "Characteristics and explanations of interference fading of a ϕ -otdr with a multi-frequency source," J. Lightwave Technol. **31**(17), 2947–2954 (2013).
21. A. H. Hartog and L. B. Liokumovich, "Phase sensitive coherent otdr with multi-frequency interrogation," (2013). US Patent App. 13/656,499.
22. D. Chen, Q. Liu, and Z. He, "Phase-detection distributed fiber-optic vibration sensor without fading-noise based on time-gated digital ofdr," Opt. Express **25**(7), 8315–8325 (2017).
23. J. Zhang, H. Wu, H. Zheng, J. Huang, G. Yin, T. Zhu, F. Qiu, X. Huang, D. Qu, and Y. Bai, "80 km fading free phase-sensitive reflectometry based on multi-carrier nlfm pulse without distributed amplification," J. Lightwave Technol. **37**(18), 4748–4754 (2019).
24. A. Hartog, L. Liokumovich, N. Ushakov, O. Kotov, T. Dean, T. Cuny, A. Constantinou, and F. Englich, "The use of multi-frequency acquisition to significantly improve the quality of fibre-optic-distributed vibration sensing," Geophys. Prospect. **66**(S1), 192–202 (2018).
25. M. Ren, P. Lu, L. Chen, and X. Bao, "Theoretical and experimental analysis of ϕ -otdr based on polarization diversity detection," IEEE Photonics Technol. Lett. **28**(6), 697–700 (2016).
26. P. J. de Groot, "Extending the unambiguous range of two-color interferometers," Appl. Opt. **33**(25), 5948–5953 (1994).
27. K. Houairi and F. Cassaing, "Two-wavelength interferometry: extended range and accurate optical path difference analytical estimator," J. Opt. Soc. Am. A **26**(12), 2503–2511 (2009).
28. B. Redding, M. J. Murray, A. Donko, M. Beresna, A. Masoudi, and G. Brambilla, "Low-noise distributed acoustic sensing using enhanced backscattering fiber with ultra-low-loss point reflectors," Opt. Express **28**(10), 14638–14647 (2020).